Enhancement of nuclear spin transitions as a resonance effect of isotope substitution

Andrey Yachmenev[1,*] and Emil Vogt[2]

[1] *Institute for Theoretical Chemistry, University of Stuttgart, Pfaffenwaldring 55, 70569 Stuttgart, Germany*
[2] *Center for Free-Electron Laser Science CFEL, Deutsches Elektronen-Synchrotron DESY, Notkestr. 85, 22607 Hamburg, Germany*

(Dated: 2025-10-27)

Mixing of different components of the total nuclear spin in the rovibrational states of isolated molecules is extremely weak. It has only been observed in hyperfine spectra for few systems, including S_2Cl_2, SiF_4, PH_3, and SF_6. We perform variational calculations of nuclear quadrupole interactions in the rotational spectra of S_2Cl_2 and CH_2Cl_2, and analyse the effects of breaking the molecular symmetry by isotopic substitution of one of the chlorine atoms. This symmetry breaking significantly enhances the mixing of nuclear spin states and produces a distinct spin polarization pattern with opposite spin orientations on the different isotopes. The enhancement arises as a resonance effect driven jointly by differences in isotopic masses and nuclear quadrupole coupling constants and gives rise to electric and magnetic dipole transitions between states with different relative orientations of the nuclear spin.

I. INTRODUCTION

Nuclear spin interactions in isolated molecules are extremely weak; hence, each rovibrational state generally has a well-defined nuclear spin component. In molecules like hydrogen or water, the nuclear spins of the two hydrogen nuclei combine to form either $I = 0$ (*para*) or $I = 1$ (*ortho*) states. These spin states impose distinct symmetry constraints on the spatial (rovibrational) part of the molecular wavefunction, resulting in different physical and chemical properties of the *ortho* and *para* forms. Such spin-induced symmetry differences enable the separation of *ortho* and *para* states in cold molecular beams using techniques like Stark deflection [1]. Similarly, in molecular collision experiments, observed differences between *ortho* and *para* states originate not from the nuclear spins themselves, but from the symmetry properties of the spatial component of the wavefunction [2]. In such contexts, nuclear spin affects molecular properties primarily by constraining the overall symmetry of the molecular quantum state.

Although mixing between nuclear spin states of different symmetry is weak, it is not strictly forbidden and can be enhanced by external perturbations, such as electric fields and radiation [3–5], molecular collisions [6–8], intermolecular interactions [9], and interactions with macromolecular environments such as surfaces or fullerenes [10, 11]. These external effects are mediated by internal nuclear hyperfine interactions between closely resonant states, commonly described by the nuclear quadrupole coupling [12, 13], magnetic spin-spin, and spin-rotation interactions [6, 14, 15]. Experimentally, purely internal mechanisms of nuclear spin-symmetry mixing have been observed through forbidden spectroscopic transitions. These include microwave transitions in S_2Cl_2, where nuclear quadrupole interactions break the nuclear spin symmetry [16], and mid-infrared transitions in SiF_4 [17], PH_3 [18], and SF_6 [19], where symmetry breaking arises from a combination of rotational energy level clustering effect and spin-rotation coupling [20].

It is an intriguing question whether internally induced mixing of nuclear spin states and the breaking of nuclear spin symmetry can produce observable effects on molecular properties. Notably, the rates of certain chemical reactions, and even enantioselectivity in electrochemical processes, have been shown to depend on the nuclear spin and magnetic moment of the reactants [21–24]. This phenomenon, known as the magnetic isotope effect, occurs when one or more atoms in a molecule are replaced by magnetic isotopes, whose nuclear spins influence chemical reactivity through hyperfine interactions with electron spins [25]. The long-lived nature of nuclear spin states is also exploited in nuclear hyperpolarization methods, which aim to enhance the sensitivity of magnetic resonance experiments [26–30]. However, to date, no connection has been established between nuclear spin symmetry breaking and either magnetic isotope effect or hyperpolarization phenomena.

In this work, we report a related effect in rotational spectra, arising from the isotopic substitution of one of two symmetry-equivalent atoms, which breaks the molecular symmetry. We investigate the symmetric molecules S_2Cl_2 and CH_2Cl_2, each containing two quadrupolar chlorine nuclei in symmetry-equivalent positions, as shown in FIG. 1. In these molecules, two off-diagonal components of the electric field gradient tensor at the chlorine nuclei change sign between the two sites. As a result, the nuclear quadrupole interaction can mix nuclear spin states of different symmetry, as previously observed and predicted in the rotational spectrum of S_2Cl_2 [13, 16]. We also predict that breaking the symmetry between the two chlorine nuclei by isotopic substitution strongly enhances this mixing, leading to nuclear spin polarization, with the two chlorine isotopes acquiring opposite spin orientations. Rotational states with opposite relative orientations of

* Email: andrey.yachmenev@theochem.uni-stuttgart.de; URL: https://github.com/robochimps

a.

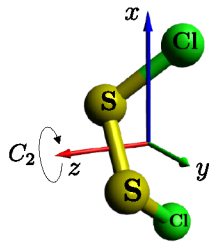

$\Gamma_{\rm rot}$	×	$\Gamma_{\rm ns}(I)$	=	$\Gamma_{\rm tot}$
A		B(0,2)		B
B		A(1,3)		B

b.

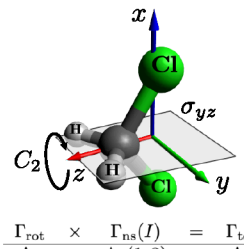

$\Gamma_{\rm rot}$	×	$\Gamma_{\rm ns}(I)$	=	$\Gamma_{\rm tot}$
A_1		$A_1(1,3)$		A_1
B_2		$B_2(0,2)$		A_1
A_2		$A_1(1,3)$		A_2
B_1		$B_2(0,2)$		A_2

FIG. 1. Equilibrium structures of S_2Cl_2 with $\mathbf{C}_2$ symmetry (a) and CH_2Cl_2 with $\mathbf{C}_{2v}$ symmetry (b) in the principal axes system oriented according to the I^r convention, where the a, b, and c axes are assigned to the z, x, and y, respectively. Also shown are the symmetry products used to construct the total spin-rotational wavefunctions, where rotational representations $\Gamma_{\rm rot}$ are combined with chlorine nuclear spin representations $\Gamma_{\rm ns}(I)$ for $I = 0, 1, 2, 3$, and only products yielding total representations $\Gamma_{\rm tot}$ that satisfy the Pauli exclusion principle are retained.

the chlorine nuclear spins have different energies and are connected by electric and magnetic dipole transitions.

This enhancement is attributed to a resonance effect arising from the combined influence of the mass difference and the change in nuclear quadrupole constants between the two chlorine isotopes. While this result may appear intuitive, to our best knowledge, this effect has not been explicitly discussed in the literature. It illustrates how even subtle changes, such as small differences in atomic mass, can significantly impact nuclear hyperfine interactions in molecules.

II. ISOTOPIC EFFECTS ON NUCLEAR-SPIN QUADRUPOLE COUPLING

The nuclear quadrupole interaction couples the rotational angular momentum $\mathbf{J}$ of a molecule with the nuclear spins of quadrupolar nuclei. For molecules containing two chlorine atoms, each with nuclear spin $I = 3/2$, the total nuclear spin angular momentum is $\mathbf{I} = \mathbf{I}_1 + \mathbf{I}_2$, leading to the possible spin quantum numbers $I = 0, 1, 2, 3$. Both S_2Cl_2 and CH_2Cl_2 possess point group symmetry operations that exchanges the two chlorine atoms, such as C_2 rotation in S_2Cl_2 and a mirror plane in CH_2Cl_2 (see FIG. 1). Nuclear spin states with $I = 0$ or 2 are antisymmetric (*para*) under chlorine exchange, while those with $I = 1$ or 3 are symmetric (*ortho*). The total angular momentum of the molecule, including nuclear spins, is denoted by $\mathbf{F} = \mathbf{J} + \mathbf{I}$.

The matrix elements of the nuclear quadrupole interaction Hamiltonian H_q in a product basis of rotational symmetric-top $|J, k\rangle$ functions and nuclear spin $|I\rangle$ functions can be written as [12, 31]

	$V_{xx,n}$	$V_{xy,n}$	$V_{xz,n}$	$V_{yy,n}$	$V_{yz,n}$	$V_{zz,n}$
$S_2^{35}Cl_2$						
^{35}Cl, $n = 1$	0.816	1.544	2.450	-1.162	1.127	0.346
^{35}Cl, $n = 2$	0.816	-1.544	-2.450	-1.162	1.127	0.346
$S_2^{35}Cl^{37}Cl$						
^{35}Cl, $n = 1$	0.849	1.560	-2.442	-1.150	-1.121	0.302
^{37}Cl, $n = 2$	0.783	-1.515	2.464	-1.184	-1.125	0.402
$CH_2^{35}Cl_2$						
^{35}Cl, $n = 1$	-0.114	0	2.481	-1.926	0	2.040
^{35}Cl, $n = 1$	-0.114	0	-2.481	-1.926	0	2.040
$CH_2^{35}Cl^{37}Cl$						
^{35}Cl, $n = 1$	-0.096	0	-2.489	-1.926	0	2.022
^{37}Cl, $n = 2$	-0.132	0	2.473	-1.926	0	2.058

TABLE I. Calculated EFG tensors $V_{\alpha\beta,n}$ (a.u.$^{-3}$) at the two chlorine nuclei ($n = 1, 2$) for the symmetric and asymmetric isotopologues of S_2Cl_2 and CH_2Cl_2 at the equilibrium geometry. The orientations of the principal x, y and z axes are shown in FIG. 1.

$$\langle F', J', k', I'|H_q|F, J, k, I\rangle = \frac{1}{\sqrt{6}}(-1)^{I'+F}\delta_{F',F} \times \sqrt{(2J'+1)(2J+1)}\begin{Bmatrix} F & I' & J' \\ 2 & J & I \end{Bmatrix} \times \sum_n^{N_q} V_n^{(J'k',Jk)}\langle I'||Q_n^{(2)}||I\rangle. \quad (1)$$

Here, $\{\cdot\}$ denotes the Wigner 6-j symbol, $V_n^{(J'k',Jk)}$ are the rotational matrix elements of the electric field gradient (EFG) tensor at nucleus n, and $\langle I'||Q_n^{(2)}||I\rangle$ are the reduced matrix elements of the quadrupole operator for that nucleus. The rotational matrix elements of the EFG tensor are given by

$$V_n^{(J'k',Jk)} = (-1)^{k'}\sum_{\sigma=-2}^{2}\begin{pmatrix} J & 2 & J' \\ k & \sigma & -k' \end{pmatrix} V_{\sigma,n}^{(2)}, \quad (2)$$

where $(\cdot)$ denotes the Wigner 3-j symbol, and $V_{\sigma,n}^{(2)}$ are components of the EFG traceless spherical tensor in the molecular frame, which is expressed in terms of Cartesian components as

$$\begin{aligned} V_{0,n}^{(2)} &= \frac{\sqrt{6}}{2}V_{zz,n}, \\ V_{\pm1,n}^{(2)} &= \mp(V_{xz,n} \pm iV_{yz,n}), \\ V_{\pm2,n}^{(2)} &= \frac{1}{2}(V_{xx,n} - V_{yy,n} \pm 2iV_{xy,n}). \end{aligned} \quad (3)$$

For a system containing two nuclei possessing identical quadrupole coupling constants, the reduced matrix elements of the quadrupole operator exhibit certain symmetry relations. In particular, when $I' - I = 0$ or ±2, the

reduced matrix elements for the two nuclei are equal,

$$\langle I, \pm 2||Q_1^{(2)}||I\rangle = \langle I, \pm 2||Q_2^{(2)}||I\rangle.$$

However, when $I' - I = \pm 1$ or ± 3, the reduced matrix elements change sign between the two nuclei,

$$\langle I \pm 1, \pm 3||Q_1^{(2)}||I\rangle = -\langle I \pm 1, \pm 3||Q_2^{(2)}||I\rangle. \quad (4)$$

Consider matrix elements of the quadrupole Hamiltonian in (1) between product states corresponding to the same rotational state but different nuclear spins, i. e., $\langle J, k, I|H_q|J, k, I'\rangle$ where $I' - I = \pm 1$ or ± 3. If rotational matrix elements of the EFG tensor are equal for both nuclei, $V_1^{(Jk,Jk)} = V_2^{(Jk,Jk)}$, then the contributions from the two nuclei to the matrix elements of H_q cancel due to the opposite sign of the corresponding reduced matrix elements in (4). The total matrix element of H_q between such states vanishes.

This cancellation occurs because the EFG tensors $V_{\alpha\beta,n}$ at the symmetry-equivalent chlorine nuclei in S_2Cl_2 and CH_2Cl_2 have identical diagonal and off-diagonal components, with some off-diagonal elements differing in sign between the two nuclei. This symmetry is evident from Table I, which lists the calculated EFG tensor components at the two chlorine nuclei in symmetric and asymmetric isotopologues of S_2Cl_2 and CH_2Cl_2. For the symmetric isotopologues, the diagonal rotational matrix elements $V_n^{(Jk,Jk)}$ are equal for $n = 1$ and 2, leading to exact cancellation of the corresponding terms in the quadrupole Hamiltonian matrix elements. The quadrupole interaction can still couple nuclear spin states with $I' - I = \pm 1$ or ± 3 (since e.g., $V_{xy,1} = -V_{xy,2}$ and $V_{xz,1} = -V_{xz,2}$), when these states belong to different rotational levels for which the symmetry conditions necessary for cancellation are no longer satisfied.

Now consider the effect of breaking molecular symmetry by substituting one of the chlorine atoms with a different isotope, replacing ^{35}Cl with ^{37}Cl. This introduces a small, yet significant, spatial asymmetry due to the change in the mass distribution. The principal axes of inertia are slightly shifted and the symmetry equivalence between the EFG tensors at the two chlorine sites is broken (see Table I). The two chlorine isotopes also have different nuclear quadrupole constants, which further contributes to the asymmetry. The matrix elements of the EFG tensors between same rotational states, $V_n^{(Jk,Jk)}$, are no longer equal for $n = 1$ and 2, so the cancellation described earlier does not occur. The off-diagonal matrix elements of the quadrupole Hamiltonian $\langle J, k, I|H_q|J, k, I'\rangle$ with $I' - I = \pm 1$ or ± 3 therefore become nonzero. Since they are comparable in magnitude to the corresponding diagonal elements $\langle J, k, I|H_q|J, k, I\rangle$, near-resonant coupling can produce strong mixing of nuclear spin states with $I' - I = \pm 1$ and ± 3.

The breaking of the molecular symmetry by isotope substitution can induce nuclear spin polarization with opposite spin orientations on the two chlorine nuclei.

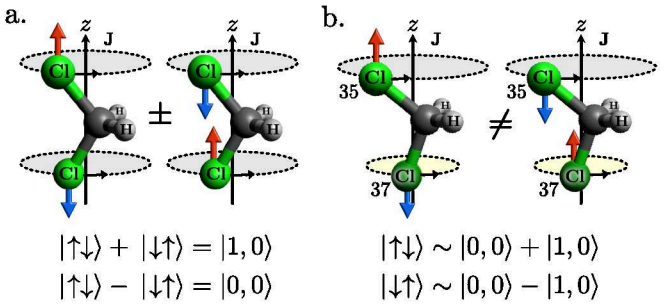

FIG. 2. (a) Energetically equivalent nuclear spin configurations for the symmetric isotopologue of $CH_2^{35}Cl_2$ rotating about its principal z-axis, resulting in well-defined *ortho* $|I = 1, m_I = 0\rangle$ and *para* $|0, 0\rangle$ nuclear spin eigenstates. (b) Energetically non-equivalent spin configurations for the asymmetric isotopologue $CH_2^{35}Cl^{37}Cl$ rotating about its principal z-axis, corresponding to broken spin symmetry and mixing of *ortho* and *para* states. The difference in rotational orbits of ^{35}Cl and ^{37}Cl in panel b is exaggerated for visual clarity.

This behavior is qualitatively different from the nuclear spin symmetry breaking in symmetric isotopologues by quadrupole interactions alone, which leads to spin polarization with the same spin orientation on both nuclei. Consider a CH_2Cl_2 molecule in a rotational state with a relatively high J quantum number and $k = J$, corresponding to classical rotation about the principal z-axis. Assume the total nuclear spin projection $m_I = 0$, such that the two chlorine nuclei have opposite spin orientations, forming total spin states with $I = 0$ (*para*) and $I = 1$ (*ortho*). In the symmetric isotopologue $CH_2^{35}Cl_2$, the two chlorine nuclei are equivalent, and the spin configurations $|\uparrow\downarrow\rangle$ and $|\downarrow\uparrow\rangle$ have identical energies, since both nuclei follow the same classical rotational orbits (see FIG. 2.a). The eigenstates of the total spin operator are then the symmetric and antisymmetric linear combinations, $\frac{1}{\sqrt{2}}(|\uparrow\downarrow\rangle \pm |\downarrow\uparrow\rangle)$, corresponding to pure *ortho* and *para* states. Consequently, in the symmetric isotopologue, the nuclear spin polarization remains identical on both chlorine nuclei, even when *ortho-para* mixing occurs between different rotational states.

In contrast, for the asymmetric isotopologue $CH_2^{35}Cl^{37}Cl$, isotopic substitution has changed the mass distribution and slightly shifted the orientation of the principal axes. The two chlorine nuclei now follow slightly different rotational trajectories, and the spin configurations $|\uparrow\downarrow\rangle$ and $|\downarrow\uparrow\rangle$ acquire slightly different energies (see FIG. 2.b). These configurations no longer correspond to pure *ortho* or *para* states but form mixtures of both. Therefore, the nuclear spin polarization can differ in sign and magnitude between the two chlorine nuclei in rotational states where *ortho-para* mixing occurs.

In symmetric isotopologues, in addition to the cancellation of certain quadrupole matrix elements due to symmetry, further constraints are imposed by the Pauli exclusion principle. For S_2Cl_2 with $\mathbf{C}_2$ symmetry, the to-

tal spin-rotational wavefunction in the ground vibrational and electronic state must transform according to the B irreducible representation. The *para* nuclear spin states ($I = 0, 2$) of B symmetry can form a symmetry-allowed product with the rotational states of A symmetry, while the *ortho* spin states ($I = 1, 3$) of A symmetry can form a product with the rotational states of B symmetry (see FIG. 1.a). For CH_2Cl_2 with $\mathbf{C}_{2v}$ symmetry, the total spin-rotational wavefunction must transform according to the A_1 or A_2 irreducible representations, due to the fermionic nature of both chlorine and hydrogen nuclei (see FIG. 1.b). Neglecting nuclear spin interactions involving the hydrogen nuclei, all combinations of rotational and nuclear spin symmetries are allowed. The statistical weights for the hydrogen nuclear spin states are 3 for total symmetries A_1 and A_2, and 1 for B_1 and B_2. In asymmetric isotopologues, molecular symmetry is reduced: for $S_2^{35}Cl^{37}Cl$ the symmetry lowers to $\mathbf{C}_1$ and for $CH_2^{35}Cl^{37}Cl$, it reduces to $\mathbf{C}_s$.

III. NUMERICAL RESULTS AND DISCUSSION

The geometries of both molecules were optimized at the CCSD(T) level (coupled-cluster singles and doubles with perturbative triples) in the frozen-core approximation, using the aug-cc-pVTZ correlation-consistent basis set [32, 33]. Dipole moments and EFG tensors were computed using coupled-cluster first-order analytical derivatives [34]. All electronic structure calculations were performed with the CFOUR quantum chemistry package [35].

Hyperfine structure calculations were carried out with the Richmol package [36] in two steps. First, rotational energies and wavefunctions were obtained by solving the Schrödinger equation with an effective Watson-type Hamiltonian, using rotational and centrifugal distortion constants determined in high-resolution spectroscopic studies [37–39]. The rotational wavefunctions were expressed as linear combinations of symmetric-top functions $|J, k, \tau\rangle$, where τ is the parity quantum number. In the second step, hyperfine states $|F, l\rangle$ (l is the hyperfine state index) were constructed as linear combinations of coupled angular momenta products of symmetry-allowed rotational wavefunctions and the joint nuclear spin functions of the chlorine nuclei $|I\rangle$. The expansion coefficients were obtained by solving the eigenvalue problem for the sum of the rotational Hamiltonian and the nuclear quadrupole interaction, as defined in (1). For the quadrupole interaction, we used *ab initio* calculated EFG tensors together with nuclear quadrupole constants $eQ(^{35}\mathrm{Cl}) = -81.65$ mb, and $eQ(^{37}\mathrm{Cl}) = -64.35$ mb [40].

The calculated nuclear quadrupole hyperfine energies and spectra for S_2Cl_2 were validated against theoretical and experimental results reported in the literature [13, 16]. All energy differences are below 1 MHz and the discrepancy is attributed to the use of *ab initio* calculated EFG tensors in the present work, as compared to the effective quadrupole coupling constants employed in previous studies [13]. The corresponding comparisons are provided in the supplementary information [41].

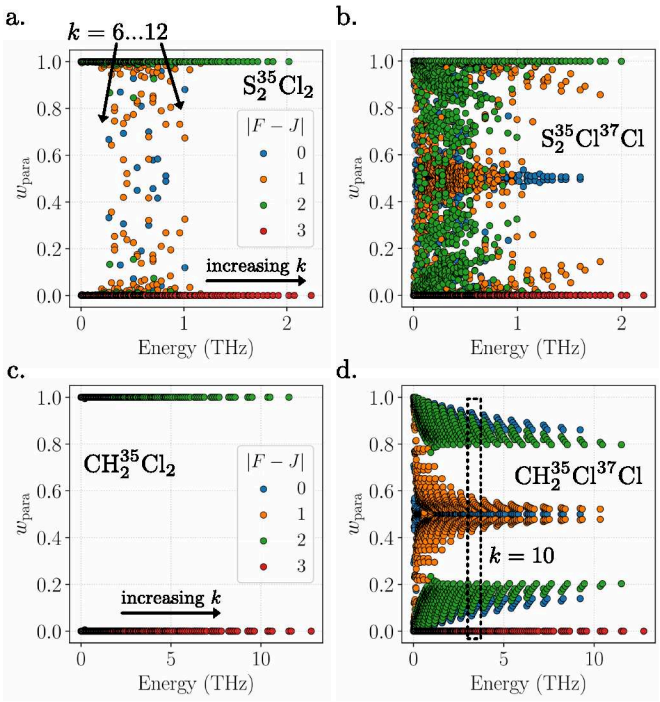

FIG. 3. Total weight of the nuclear spin *para* ($I = 0, 2$) contributions to rotational states as a function of the state energy for symmetric and asymmetric isotopologues of S_2Cl_2 (panels a, b) and CH_2Cl_2 (panels c, d). The *para* weights w_{para} are calculated as the sum of squares of the wavefunction linear expansion coefficients corresponding to basis states $|J, k, \tau\rangle|I = 0\rangle$ or $|J, k, \tau\rangle|I = 2\rangle$. The weight of the *ortho* contributions ($I = 1, 3$) is given by $w_{\mathrm{ortho}} = 1 - w_{\mathrm{para}}$. States are color-coded by the quantum number difference $|F - J|$.

To analyze the mixing of nuclear spin states, we calculated the total weight w_{para} of contributions from nuclear spins $I = 0$ and 2 (*para*) to each rotational state. The complementary contribution from nuclear spins with $I = 1$ and 3 (*ortho*) is given by $w_{\mathrm{ortho}} = 1 - w_{\mathrm{para}}$. The results for symmetric and asymmetric isotopologues of S_2Cl_2 and CH_2Cl_2 are shown in FIG. 3 for all rotational states with $F \leq 17$ ($J \leq 20$). As both molecules are close to prolate tops (Ray's asymmetry parameter $\kappa < -0.9$), groups of rotational states with increasing energy correspond to increasing values of the rotational quantum number k. In the symmetric isotopologue of S_2Cl_2 (FIG. 3.a), significant *ortho-para* mixing is observed only for states with $k = 6..12$ ($J = 9..18$). In contrast, the symmetric isotopologue of CH_2Cl_2 (FIG. 3.c) exhibits no noticeable *ortho-para* mixing.

For the asymmetric isotopologues, strong *ortho-para* mixing occurs across all k-values. The effect is more pronounced in S_2Cl_2 than in CH_2Cl_2, which can be attributed to its lower molecular symmetry, for example, the presence of all nonzero off-diagonal components in the EFG tensor (Table I). In CH_2Cl_2, symmetry constraints

J	k	τ	I	F	m_F	E (MHz)	w_{para}	w_{ortho}	$\langle\hat{I}_{Z,1}\rangle$	$\langle\hat{I}_{Z,2}\rangle$
$S_2^{35}Cl_2$										
12	7	0	3	9	9	411775.0324	0.00	1.00	-1.350	-1.350
12	7	0	1	12	12	411775.0468	0.24	0.76	0.056	0.056
12	7	1	2	12	12	411775.0469	0.76	0.24	0.059	0.059
12	7	0	3	15	15	411775.0599	0.00	1.00	1.500	1.500
12	7	0	3	10	10	411775.1206	0.00	1.00	-0.773	-0.773
12	7	1	2	11	11	411775.1407	0.51	0.49	-0.363	-0.363
12	7	1	2	11	11	411775.1437	0.49	0.51	-0.361	-0.361
$S_2^{35}Cl^{37}Cl$										
10	10	1	3	7	7	560199.1545	0.00	1.00	-1.312	-1.312
10	10	1	3	8	8	560201.3164	0.01	0.99	-0.647	-0.799
10	10	0	2	8	8	560202.1378	0.99	0.01	-0.964	-0.812
10	10	0	3	9	9	560202.0034	0.21	0.79	0.484	-1.120
10	10	0	2	9	9	560202.1712	0.79	0.21	-1.142	0.460
10	10	1	1	10	10	560199.5391	0.49	0.51	1.496	-1.358
10	10	0	1	10	10	560199.5581	0.51	0.49	-1.358	1.495
$CH_2^{35}Cl^{37}Cl$										
10	10	0	3	7	7	3214525.1465	0.00	1.00	-1.312	-1.312
10	10	0	3	8	8	3214537.3502	0.09	0.91	-1.032	-0.442
10	10	0	2	8	8	3214543.1327	0.91	0.09	-0.579	-1.169
10	10	0	2	9	9	3214540.4378	0.43	0.57	-1.297	0.641
10	10	0	2	9	9	3214544.2488	0.57	0.43	0.635	-1.297
10	10	0	1	10	10	3214527.2361	0.50	0.50	-1.357	1.496
10	10	1	1	10	10	3214527.7134	0.50	0.50	1.494	-1.359

TABLE II. Expectation values of the nuclear spin operators $\hat{I}_{Z,n}$ $(n = 1, 2)$ for the two chlorine atoms in selected hyperfine states of symmetric $S_2^{35}Cl_2$ and asymmetric $S_2^{35}Cl^{37}Cl$ isotopologues of S_2Cl_2, as well as the asymmetric $CH_2^{35}Cl^{37}Cl$ isotopologue. Results for the symmetric isotopologue of $CH_2^{35}Cl_2$ are omitted, as it exhibits no significant *ortho-para* mixing (see FIG. 3.c).

allow only the V_{xz} nonzero off-diagonal component. Additionally, isotopic substitution of one chlorine atom in S_2Cl_2 induces a larger asymmetry in the diagonal components of the EFG tensor between the two chlorine atoms compared to CH_2Cl_2, due to a larger shift of the principal axes. For $S_2^{35}Cl^{37}Cl$, the differences $V_{\alpha\alpha}(^{35}\text{Cl}) - V_{\alpha\alpha}(^{37}\text{Cl})$ are 0.07, 0.03, and -0.10 a.u.$^{-3}$ for $\alpha = x, y, z$, respectively (see Table I). The corresponding values for CH_2Cl_2 are smaller: 0.04, 0.0, and -0.04 a.u.$^{-3}$.

We did not find a clear correlation between the strong mixing of nuclear spin states in rotational levels and specific combinations of quantum numbers or characteristic features of the rotational probability density distributions. However, some states with quantum number differences $|F - J| = 0$ and 1 appear to exhibit the strongest mixing.

To investigate the nuclear spin polarization effect, we calculated the expectation values of the chlorine nuclear spin operators, $\langle F, m_F, l|\hat{I}_{Z,n}|F, m_F, l\rangle$ $(n = 1, 2)$, listed in Table II, together with the corresponding laboratory-frame spin-density distributions, $\rho_n^{(F,m_F,l)}$, shown in FIG. 4, for selected J, k rotational branch and with

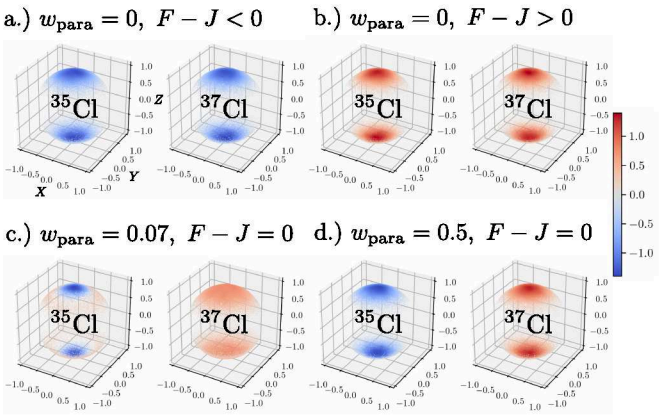

FIG. 4. Nuclear spin density distributions for the laboratory-frame Z-component of the ^{35}Cl and ^{37}Cl nuclear spins in the asymmetric isotopologue $CH_2^{35}Cl^{37}Cl$, represented in Cartesian coordinates on a unit sphere. Results are shown for selected rotational states with quantum numbers $J = 10$ and $k = 10$ ($m_F = F$), indicated by the dashed rectangle in FIG. 3.d. Four specific cases are shown: (a) a pure *ortho* state ($w_{\text{para}} = 0$) with $F - J < 0$; (b) a pure *ortho* state with $F - J > 0$; (c) a mostly *ortho* state ($w_{\text{para}} \gtrsim 0$) with $F - J = 0$; (d) a state with equal *ortho* and *para* contributions ($w_{\text{para}} = 0.5$) with $F - J = 0$.

$m_F = F$. Data for other states are available in the supplementary information [41]. The spin-density is defined as

$$\rho_n^{(F,m_F,l)}(\mathbf{r}_g) = \langle F, m_F, l|\delta(\mathbf{r}_n - \mathbf{r}_g)\hat{I}_{Z,n}|F, m_F, l\rangle,$$

where l indexes the hyperfine states with the total angular momentum quantum number F, $\mathbf{r}_n$ denotes the normalized Cartesian coordinate of the nth chlorine nucleus, and $\mathbf{r}_g$ is the laboratory-frame position mapped onto a unit sphere. Evaluating this function on a grid of $\mathbf{r}_g$ values yields the probability density of the nuclear spin being oriented 'up' or 'down' along the laboratory Z-axis as a function of the angular position of nucleus n. To generate the distributions, we sample molecular orientations $\mathbf{r}_g$ using a rejection-sampling approach, with the absolute value of ρ_n taken as the sampling weight.

The density plots in FIG. 4 correspond to states with $m_F = F$, which classically represents a molecule rotating about an axis that precesses around the laboratory Z-axis, with the axis becoming increasingly aligned with Z for larger F. For each chlorine nucleus, the plots demonstrate alignment close to the Z-axis, with equal probability of finding one nucleus in the upper hemisphere and the other in the lower, or vice versa. The color scale indicates the projection of each nuclear spin onto the Z-axis.

As expected, in symmetric isotopologues the spin operators and densities show the same nuclear spin orientation and magnitude for both chlorine nuclei, even in states with strong *ortho-para* mixing. The direction of spin polarization, positive or negative, is determined by the sign of the difference between the total and rotational angular momentum quantum numbers, $F - J$. A similar behavior

is predicted for asymmetric isotopologues in pure *ortho* or *para* states, where both chlorine nuclei also exhibit identical nuclear spin magnitudes and orientation. This is illustrated in FIG. 4.a and FIG. 4.b for the $k = J = 10$ states of $CH_2^{35}Cl^{37}Cl$. In contrast, for mixed *ortho-para* states of asymmetric isotopologues ($0 < w_{\text{para}} < 1$), the spin operators and densities reveal opposite spin orientations on the two chlorine nuclei, as shown in FIG. 4.c and FIG. 4.d. For states with unequal *ortho-para* mixing ($w_{\text{para}} \neq 0.5$), the magnitudes of the nuclear spin polarization on the two nuclei also differ. A similar pattern is predicted for the $S_2^{35}Cl^{37}Cl$ isotopologue.

The existence of states with broken spin symmetry, where different relative orientations of the nuclear spins are associated with different field-free energies, enables spin-flipping transitions via electric or magnetic dipole interactions with external fields. Moreover, additional electric-dipole transition pathways become allowed in asymmetric isotopologues as a result of symmetry breaking. Such spin-switching transitions may be of interest for applications such as quantum information processing [42].

As an example, consider the state $|J, k, \tau, I, F\rangle = |2, 2, 1, 1, 2\rangle$ of $CH_2^{35}Cl^{37}Cl$ with energy 133716.7 MHz that has nuclear spin expectation values of $\langle \hat{I}_{1,Z} \rangle = -0.62$ for ^{35}Cl and $\langle \hat{I}_{2,Z} \rangle = 1.40$ for ^{37}Cl. This state is connected via a magnetic dipole transition to $|2, 2, 1, 0, 2\rangle$ at 133718.3 MHz, which has flipped nuclear spin orientations, with $\langle \hat{I}_{1,Z} \rangle = 1.31$ and $\langle \hat{I}_{2,Z} \rangle = -0.76$. The magnetic dipole moment is defined as $\hat{d}_Z = \mu_N(g_1 \hat{I}_{Z,1} + g_2 \hat{I}_{Z,2})$, where g_n are the nuclear g-factors [43] and μ_N is the nuclear magneton. For the transition between the states above, the calculated magnetic dipole matrix element is $0.11\mu_N$. In addition, a weak electric dipole transition connects the same initial state to its opposite-parity counterpart $|2, 2, 0, 0, 2\rangle$, which also exhibits flipped nuclear spin orientations. The corresponding transition matrix element is $\langle \mu_Z \rangle \approx i10^{-4}$ a.u., a coupling that is absent in the symmetric isotopologue.

An extensive list of electric- and magnetic-dipole spin-switching transitions originating from states with opposite nuclear spin orientations at different chlorine nuclei in $CH_2^{35}Cl^{37}Cl$ and $S_2^{35}Cl^{37}Cl$ is provided in the supplementary information [41]. Some of these transitions exhibit relatively large electric dipole moments, on the order of 10^{-1} a.u, and may be exploited in electrical schemes for controlling nuclear spin dynamics [44, 45].

Finally, we simulated the absorption spectra at $T = 10$ K for symmetric and asymmetric isotopologues of S_2Cl_2 and CH_2Cl_2, as shown in FIG. 5. The transitions are grouped by $\Delta I = |I' - I|$ with $\Delta I = 0, 2$ (*ortho-ortho* and *para-para*) and $\Delta I = 1, 3$ (*ortho-para*) and shown with different colors. However, this classification becomes somewhat ambiguous for the asymmetric isotopologues when *ortho* and *para* states are strongly mixed. Therefore, we highlight in red the transitions for which one or both states exhibit strong *ortho-para* mixing, with $0.4 < w_{\text{para}} < 0.6$. Notably, all strong transitions assigned as *ortho-para* (indicated by red circles) occur between such strongly mixed states. In the asymmetric isotopologues, the presence of additional allowed energy levels increases the partition function compared to the symmetric isotopologues. This reduces the population of the individual initial states, making the strongest transitions appear weaker than the corresponding transitions of the symmetric isotopologues.

The experimentally observed forbidden *ortho-para* transitions in $S_2^{35}Cl_2$ [16] occur near 12 000 MHz, with intensities between 10^{-3} and 10^{-4} times weaker than the allowed transitions in this region. As shown in FIG. 5.a, however, $S_2^{35}Cl_2$ also exhibits forbidden *ortho-para* transitions at higher frequencies that are of the same order of magnitude as the allowed ones. For $CH_2^{35}Cl_2$, the forbidden transitions are much weaker than in $S_2^{35}Cl_2$ and therefore are not visible in the linear-scale spectrum shown in FIG. 5.c. Nonetheless, the strongest transitions in the 10 000–20 000 MHz range reach intensities about 10^{-3} relative to the allowed ones (see supplementary information [41]).

As expected, the forbidden transitions ($\Delta I = 1, 3$) shown in Figure FIG. 5 for the symmetric isotopologues are generally significantly weaker than the allowed transitions ($\Delta I = 0, 2$). In the depicted region, the ratio between the strongest $\Delta I = 1, 3$ and $\Delta I = 0, 2$ transitions is only $\sim 10^{-3}$ for $CH_2^{35}Cl_2$. In constast, for the asymmetric isotopologue, $CH_2^{35}Cl^{37}Cl$, this ratio is about 0.5. For S_2Cl_2, the strongest $\Delta I = 1, 3$ and $\Delta I = 0, 2$ transitions are of similar magnitude (ratio of ~ 0.5) for both the symmetric and asymmetric isotopologue. However, several strong $\Delta I = 1, 3$ transitions are predicted for $S_2^{35}Cl^{37}Cl$, and the $\Delta I = 1, 3$ transitions contribute more than 4% of the total intensity in the shown spectral region.

We believe this phenomenon can be experimentally observed through high-resolution spectra, for example by fitting effective Hamiltonians that include hyperfine interactions [16, 37, 46]. In particular, comparison of the experimental and simulated spectra of $S_2^{35}Cl^{37}Cl$ (Fig. 3.b in [46]) with our calculations suggest the presence of weak *ortho-para* transitions within the $J_{k_a,k_c} = 2_{20} - 1_{11}$ rotational transition band (see the supplementary materials).

It should be emphasized that, since the effect originates from resonances, the hyperfine line positions and especially the intensities of the *ortho-para* transitions are highly sensitive to both the effective rotational constants and the accuracy of the quadrupole coupling constants. In first-principles approaches, it is therefore essential to include centrifugal and Coriolis interactions. As a result, the overall accuracy depends on both the quality of the potential energy surface near equilibrium and the accuracy of the calculated electric field gradient tensors.

IV. CONCLUSIONS

We demonstrated that isotope substitution in CH_2Cl_2 and S_2Cl_2 molecules with strong nuclear quadrupole cou-

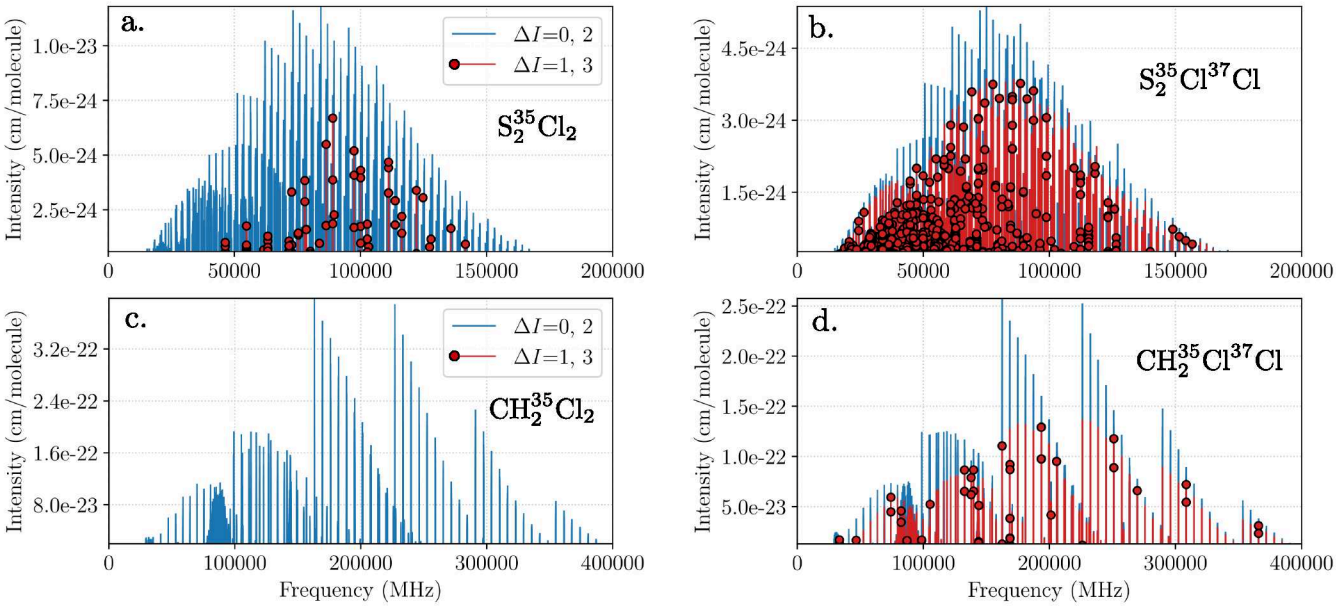

FIG. 5. Hyperfine rotational absorption spectra of symmetric and asymmetric S_2Cl_2 isotopologues (panels a, b) and symmetric and asymmetric $CH_2^{35}Cl_2$ isotopologues (panels b, c), calculated for all states with $F \leq 17$ ($J \leq 20$) and $T = 10$ K. Transitions involving states with strong *ortho-para* mixing ($0.4 < w_{\text{para}} < 0.6$) are shown in red. Transitions between states differing in total nuclear spin by 1 or 3 (based on the assignment by leading basis contribution) are emphasized with red circles.

pling breaks nuclear spin symmetry and significantly enhances the mixing of nuclear spin states, producing spin polarization with opposite orientations on different isotopic nuclei. In the literature, isotope substitution has been discussed in terms of mass-dependent effects and hyperfine interactions with electron spins [23, 25]. Here, we highlight an additional possible mechanism: isotopes acquiring opposite nuclear spin orientations. Since nuclear spin polarization was observed to remain relatively stable following processes such as photodissociation or dissociative ionization [27, 47], opposite-sign polarization between isotopes could also influence chemical reactivity, particularly in external magnetic fields where subtle energy shifts arise depending on spin orientation.

We further show that isotope substitution can enhance forbidden *ortho-para* transitions by orders of magnitude, from $\sim 10^{-3}$ in the symmetric isotopologue, CH_2Cl_2, to ~ 0.5 in the asymmetric isotopologue $CH_2^{35}Cl^{37}Cl$. With such strong mixing, the distinction between *ortho* and *para* states becomes less meaningful. However, an interesting observation is that many of the enhanced transitions connect rotational states with opposite relative orientations of nuclear spins on the two chlorine nuclei. These transitions may provide new pathways for controlling nuclear spin dynamics. In addition, nuclear spin polarization offers a sensitive probe for high-resolution spectroscopy and precision measurements, for example, in studies of parity violation associated with chirality induced by isotope substitution, such as in $CHFCl_2$, where nuclear-spin-dependent contributions may play a significant role [48–50].

V. SUPPLEMENTARY MATERIAL

The supplementary material includes an archived snapshot on the repository `https://github.com/robochimps/isotope_nqr`, which contains all Python code required to reproduce and extend the results of this study. In particular, the Jupyter notebook files `s2cl2_35_35.ipynb`, `s2cl2_35_37.ipynb`, `ch2cl2_35_35.ipynb`, and `ch2cl2_35_37.ipynb` provide the results of calculations for $S_2^{35}Cl_2$, $S_2^{35}Cl^{37}Cl$, $CH_2^{35}Cl_2$, and $CH_2^{35}Cl^{37}Cl$, respectively.

VI. DATA AVAILABILITY

The complete code and calculation results supporting this study are provided in Jupyter notebook format in the following repository: `https://github.com/robochimps/isotope_nqr`.

VII. CODE AVAILABILITY

The `Richmol` computer code developed and used in this work is available at: `https://github.com/robochimps/richmol`.

VIII. ACKNOWLEDGEMENTS

The work of EV was supported by the European Union's Horizon Europe research and innovation programme under Marie Skłodowska-Curie grant agreement No. 101155136, and by the Deutsches Elektronen-Synchtrotron DESY, a member of the Helmholtz Association (HGF).

[1] D. A. Horke, Y. Chang, K. Długołęcki, and J. Küpper, Separating para and ortho water, Angew. Chem. Int. Ed. **53**, 11965 (2014).

[2] A. Kilaj, H. Gao, D. Rösch, U. Rivero, J. Küpper, and S. Willitsch, Observation of different reactivities of para and ortho-water towards trapped diazenylium ions, Nat. Commun. **9**, 2096 (2018).

[3] B. Nagels, N. Calas, D. A. Roozemond, L. J. F. Hermans, and P. L. Chapovsky, Level-crossing resonances in nuclear spin conversion of molecules, Phys. Rev. Lett. **77**, 4732 (1996).

[4] P. L. Chapovsky, Hyperfine spectra of CH_3F nuclear spin conversion, J. Phys. B **33**, 1001 (2000).

[5] P. L. Chapovsky, Conversion of nuclear spin isomers of water molecules under ultracold conditions of space, Quantum Electron. **49**, 473 (2019).

[6] P. L. Chapovsky and L. J. F. Hermans, Nuclear spin conversion in polyatomic molecules, Annu. Rev. Phys. Chem. **50**, 315 (1999).

[7] Z.-D. Sun, K. Takagi, and F. Matsushima, Separation and conversion dynamics of four nuclear spin isomers of ethylene, Science **310**, 1938 (2005).

[8] Z.-D. Sun, M. Ge, and Y. Zheng, Separation and conversion dynamics of nuclear-spin isomers of gaseous methanol, Nat. Comm. **6**, 6877 (2015).

[9] T. Meier, D. Laniel, M. Pena-Alvarez, F. Trybel, S. Khandarkhaeva, A. Krupp, J. Jacobs, N. Dubrovinskaia, and L. Dubrovinsky, Nuclear spin coupling crossover in dense molecular hydrogen, Nat. Comm. **11**, 6334 (2020).

[10] B. Meier, S. Mamone, M. Concistrè, J. Alonso-Valdesueiro, A. Krachmalnicoff, R. J. Whitby, and M. H. Levitt, Electrical detection of ortho-para conversion in fullerene-encapsulated water, Nat. Comm. **6**, 8112 (2015).

[11] C. Beduz, M. Carravetta, J. Y.-C. Chen, M. Concistrè, M. Denning, M. Frunzi, A. J. Horsewill, O. G. Johannessen, R. Lawler, X. Lei, M. H. Levitt, Y. Li, S. Mamone, Y. Murata, U. Nagel, T. Nishida, J. Ollivier, S. Rols, T. Rõõm, R. Sarkar, N. J. Turro, and Y. Yang, Quantum rotation of ortho and para-water encapsulated in a fullerene cage, Proc. Natl. Acad. Sci. U.S. A. **109**, 12894 (2012).

[12] A. Yachmenev and J. Küpper, Communication: General variational approach to nuclear-quadrupole coupling in rovibrational spectra of polyatomic molecules, J. Chem. Phys. **147**, 141101 (2017), arXiv:1709.08558 [physics].

[13] G. Wichmann, G. Seyfang, and M. Quack, Time-dependent dynamics of nuclear spin symmetry and parity violation in dichlorodisulfane (ClSSCl) during and after coherent radiative excitation, Mol. Phys. **119**, e1959073 (2021).

[14] A. Miani and J. Tennyson, Can ortho-para transitions for water be observed?, J. Chem. Phys. **120**, 2732 (2004).

[15] A. Yachmenev, G. Yang, E. Zak, S. Yurchenko, and J. Küpper, The nuclear-spin-forbidden rovibrational transitions of water from first principles, J. Chem. Phys. **156**, 204307 (2022).

[16] H. Kanamori, Z. T. Dehghani, A. Mizoguchi, and Y. Endo, Detection of microwave transitions between ortho and para states in a free isolated molecule, Phys. Rev. Lett. **119**, 173401 (2017).

[17] O. Pfister, C. Chardonnet, and C. J. Bordé, Hyperfine-induced lifting of parity degeneracy in noninverting molecules, Phys. Rev. Lett. **76**, 4516 (1996).

[18] R. J. Butcher, Ch. Chardonnet, and Ch. J. Bordé, Hyperfine lifting of parity degeneracy and the question of inversion in a rigid molecule, Phys. Rev. Lett. **70**, 2698 (1993).

[19] J. Bordé, Ch. J. Bordé, C. Salomon, A. Van Lerberghe, M. Ouhayoun, and C. D. Cantrell, Breakdown of the point-group symmetry of vibration-rotation states and optical observation of ground-state octahedral splittings of $^{32}SF_6$ using saturation spectroscopy, Phys. Rev. Lett. **45**, 14 (1980).

[20] A. Yachmenev and G. Yang, Nuclear spin symmetry breaking and spin polarization in rotational energy level clusters, Phys. Rev. Research **7**, L032047 (2025), arXiv:2503.20695 [physics].

[21] A. L. Buchachenko, Magnetic isotope effect: Nuclear spin control of chemical reactions, J. Phys. Chem. A **105**, 9995 (2001).

[22] L. C. Motta, A. D. Chien, A. E. Rask, and P. M. Zimmerman, Mercury magnetic isotope effect: A plausible photochemical mechanism, J. Phys. Chem. A **124**, 3711 (2020).

[23] Y. Kim, F. Bertagna, E. M. D'Souza, D. J. Heyes, L. O. Johannissen, E. T. Nery, A. Pantelias, A. Sanchez-Pedreño Jimenez, L. Slocombe, M. G. Spencer, J. Al-Khalili, G. S. Engel, S. Hay, S. M. Hingley-Wilson, K. Jeevaratnam, A. R. Jones, D. R. Kattnig, R. Lewis, M. Sacchi, N. S. Scrutton, S. R. P. Silva, and J. McFadden, Quantum biology: An update and perspective, Quant. Rep. **3**, 80 (2021).

[24] O. Vardi, N. Maroudas-Sklare, Y. Kolodny, A. Volosniev, A. Saragovi, N. Galili, S. Ferrera, A. Ghazaryan, N. Yuran, H. P. Affek, B. Luz, Y. Goldsmith, N. Keren, S. Yochelis, I. Halevy, M. Lemeshko, and Y. Paltiel, Nuclear spin effects in biological processes, PNAS **120**, e2300828120 (2023).

[25] C. T. Rodgers, Magnetic field effects in chemical systems, Pure Appl. Chem. **81**, 19 (2009).

[26] C. R. Bowers and D. P. Weitekamp, Parahydrogen and synthesis allow dramatically enhanced nuclear alignment, J. Am. Chem. Soc. **109**, 5541 (1987).

[27] T. P. Rakitzis, Highly spin-polarized atoms and molecules from rotationally state-selected molecules, Phys. Rev. Lett. **94**, 083005 (2005).

[28] B. Meier, J.-N. Dumez, G. Stevanato, J. T. Hill-Cousins, S. S. Roy, P. Håkansson, S. Mamone, R. C. D. Brown, G. Pileio, and M. H. Levitt, Long-lived nuclear spin states in methyl groups and quantum-rotor-induced polarization, J. Am. Chem. Soc. **135**, 18746 (2013).

[29] J.-N. Dumez, P. Håkansson, S. Mamone, B. Meier, G. Stevanato, J. T. Hill-Cousins, S. S. Roy, R. C. D. Brown, G. Pileio, and M. H. Levitt, Theory of long-lived nuclear spin states in methyl groups and quantum-rotor induced polarisation, J. Chem. Phys. **142**, 044506 (2015).

[30] J. Eills, D. Budker, S. Cavagnero, E. Y. Chekmenev, S. J. Elliott, S. Jannin, A. Lesage, J. Matysik, T. Meersmann, T. Prisner, J. A. Reimer, H. Yang, and I. V. Koptyug, Spin hyperpolarization in modern magnetic resonance, Chem. Rev. **123**, 1417 (2023).

[31] R. L. Cook and F. C. De Lucia, Application of the theory of irreducible tensor operators to molecular hyperfine structure, Am. J. Phys. **39**, 1433 (1971).

[32] T. H. Dunning, Gaussian basis sets for use in correlated molecular calculations. I. The atoms boron through neon and hydrogen, J. Chem. Phys. **90**, 1007 (1989).

[33] R. A. Kendall, T. H. Dunning, Jr., and R. J. Harrison, Electron affinities of the first-row atoms revisited. Systematic basis sets and wave functions, J. Chem. Phys. **96**, 6796 (1992).

[34] G. E. Scuseria, Analytic evaluation of energy gradients for the singles and doubles coupled cluster method including perturbative triple excitations: Theory and applications to FOOF and Cr_2, J. Chem. Phys. **94**, 442 (1991).

[35] J. F. Stanton, J. Gauss, L. Cheng, M. E. Harding, D. A. Matthews, and P. G. Szalay, CFOUR, Coupled-Cluster techniques for Computational Chemistry, a quantum-chemical program package, With contributions from A.A. Auer, R.J. Bartlett, U. Benedikt, C. Berger, D.E. Bernholdt, S. Blaschke, Y. J. Bomble, S. Burger, O. Christiansen, D. Datta, F. Engel, R. Faber, J. Greiner, M. Heckert, O. Heun, M. Hilgenberg, C. Huber, T.-C. Jagau, D. Jonsson, J. Jusélius, T. Kirsch, K. Klein, G.M. KopperW.J. Lauderdale, F. Lipparini, T. Metzroth, L.A. Mück, D.P. O'Neill, T. Nottoli, D.R. Price, E. Prochnow, C. Puzzarini, K. Ruud, F. Schiffmann, W. Schwalbach, C. Simmons, S. Stopkowicz, A. Tajti, J. Vázquez, F. Wang, J.D. Watts and the integral packages MOLECULE (J. Almlöf and P.R. Taylor), PROPS (P.R. Taylor), ABACUS (T. Helgaker, H.J. Aa. Jensen, P. Jørgensen, and J. Olsen), and ECP routines by A. V. Mitin and C. van Wüllen. For the current version, see http://www.cfour.de.

[36] A. Yachmenev, Richmol: Python package for variational simulations of molecular nuclear motion dynamics in fields (2025), available at: `https://github.com/robochimps/richmol`.

[37] Z. T. Dehghani, S. Ota, A. Mizoguchi, and H. Kanamori, Millimeter-wave spectroscopy of S_2Cl_2: A candidate molecule for measuring ortho-para transition, J. Phys. Chem. A **117**, 10041 (2013).

[38] O. Ulenikov, O. Gromova, E. Bekhtereva, H. Müller, and L. Margulès, Submillimeter wave spectrum of methylene chloride, $^{12}CH_2^{35}Cl_2$, $^{12}CH_2^{35}Cl^{37}Cl$ and $^{12}CH_2^{37}Cl_2$ up to 1.1 THz, J. Quant. Spectrosc. Radiat. Transf. **319**, 108962 (2024).

[39] M. Kobayashi, K. Kobayashi, B. J. Esselman, R. Woods, R. J. McMahon, S. Yamamoto, and H. Ozeki, The rotational spectroscopy of dichloromethane ($CH_2^{35}Cl_2$) in the ground state and ν_4 vibrationally excited state from 11 to 750 GHz, J. Mol. Spectrosc. **407**, 111982 (2025).

[40] P. Pyykkö, Year-2008 nuclear quadrupole moments, Mol. Phys. **106**, 1965 (2008).

[41] E. V. Andrey Yachmenev, Isotope_nqr: Effects of isotope substitution on nuclear-quadrupole hyperfine interactions (2025), available at: `https://github.com/robochimps/isotope_nqr`.

[42] K. Saeedi, S. Simmons, J. Z. Salvail, P. Dluhy, H. Riemann, N. V. Abrosimov, P. Becker, H.-J. Pohl, J. J. L. Morton, and M. L. W. Thewalt, Room-temperature quantum bit storage exceeding 39 minutes using ionized donors in silicon-28, Science **342**, 830 (2013).

[43] N. Stone, Table of nuclear magnetic dipole and electric quadrupole moments, At. Data Nucl. Data Tables **90**, 75 (2005).

[44] R. Savytskyy, T. Botzem, I. Fernandez de Fuentes, B. Joecker, J. J. Pla, F. E. Hudson, K. M. Itoh, A. M. Jakob, B. C. Johnson, D. N. Jamieson, A. S. Dzurak, and A. Morello, An electrically driven single-atom "flip-flop" qubit, Science Adv. **9**, eadd9408 (2023).

[45] H. Xu, C. Li, G. Wang, H. Wang, H. Tang, A. R. Barr, P. Cappellaro, and J. Li, Two-photon interface of nuclear spins based on the optonuclear quadrupolar effect, Phys. Rev. X **13**, 011017 (2023).

[46] A. Mizoguchi, S. Ota, H. Kanamori, Y. Sumiyoshi, and Y. Endo, Analysis of the nuclear quadrupole interaction of disulfur dichloride, S_2Cl_2, J. Mol. Spectrosc. **250**, 86 (2008).

[47] D. Sofikitis, L. Rubio-Lago, M. R. Martin, D. J. A. Brown, N. C.-M. Bartlett, R. N. Zare, and T. P. Rakitzis, Preparation of highly polarized nuclei: Observation and control of time-dependent polarization transfer from $H^{35}Cl$ molecular rotation to ^{35}Cl nuclear spin, Physical Review A **76**, 012503 (2007).

[48] D. DeMille, S. B. Cahn, D. Murphree, D. A. Rahmlow, and M. G. Kozlov, Using molecules to measure nuclear spin-dependent parity violation, Phys. Rev. Lett. **100**, 023003 (2008).

[49] I. A. Aucar, Y. Chamorro, and A. Borschevsky, Parity-violating contributions to nuclear spin-rotation interactions and to NMR shielding constants in tetrahedral molecules, Phys. Rev. A **106**, 062802 (2022).

[50] R. Bast, P. Schwerdtfeger, and T. Saue, Parity nonconservation contribution to the nuclear magnetic resonance shielding constants of chiral molecules: A four-component relativistic study, J. Chem. Phys. **125**, 064504 (2006).